An MLE of Interferometric Coherence Matrix and its Applications in Multipolarimetric Interferometric Phase Optimization and Phase Series Estimation

Guobing Zeng, Huaping Xu, *Member, IEEE*, Wei Liu, *Senior Member, IEEE*, Aifang Liu, and Yuan Wang

***Abstract*—Multipolarimetric synthetic aperture radar (SAR) interferometric phase optimization and phase series estimation have received a lot of attentions recently from the polarimetry SAR interferometry (PolInSAR) community. In this article, a maximum likelihood estimation (MLE) method for the interferometric coherence matrix (ICM) is proposed, which is further applied to both interferometric phase optimization and phase series estimation. By modeling the PolInSAR coherence matrix as the Kronecker product of the polarimetric coherence matrix and ICM, the MLE of ICM under complex circular Gaussian distribution hypothesis is acquired through an alternate iterative optimization method. In addition, it is theoretically proved in this article that the two state-of-the-art methods, i.e., the TP (total power) method and the MLE-MPPL method, are suboptimal compared to the proposed method regarding the MLE of ICM. Numerical experiments are conducted on simulated fully polarimetric data, airborne fully polarimetric E-SAR data, and spaceborne dual polarimetric Sentinel-1A data, to confirm the effectiveness and superiority of the proposed method.**

***Index Terms*—Interferometric coherence matrix (ICM), interferometric phase optimization, maximum likelihood estimation (MLE), phase series estimation, PolInSAR.**

Nomenclature

CCG	Complex circular Gaussian.
DEM	Digital elevation model.
ESPO	Exhaustive search polarimetric optimization.
EMI	Eigendecomposition-based maximum-likelihood-estimator of interferometric phase.
EVD	Eigenvalue decomposition.
ICM	Interferometric coherence matrix.
MLE-MPPL	Maximum likelihood estimator for multipolarimetric phase-linking.
MLE	Maximum likelihood estimation.
PCM	Polarimetric coherence matrix.
PolSAR	Polarimetric SAR.
PolInSAR	Polarimetric SAR interferometry.
RMSE	Root-mean-square error.
SKP	Sum of Kronecker product.
TP	Total power.

Manuscript received 14 August 2023; revised 10 October 2023; accepted 20 October 2023. Date of publication 24 October 2023; date of current version 14 November 2023. This work was supported in part by the National Natural Science Foundation of China under Grant U2241202. *(Corresponding author: Huaping Xu.)*

Guobing Zeng, Huaping Xu, and Yuan Wang are with the School of Electronic and Information Engineering, Beihang University, Beijing 100191, China (e-mail: zengguobing@buaa.edu.cn; xuhuaping@buaa.edu.cn; wyuan@buaa.edu.cn).

Wei Liu is with the Department of Electronic Engineering and Computer Science, Queen Mary University of London, E1 4NS London, U.K. (e-mail: w.liu@qmul.ac.uk).

Aifang Liu is with the China Electronics Technology Group Corporation 14th Research Institute, Nanjing 210000, China (e-mail: lafsx1997@163.com).

Digital Object Identifier 10.1109/JSTARS.2023.3327196

I. Introduction

THE polarimetric capability of synthetic aperture radar (SAR) sensors has offered huge potentials for PolSAR and PolInSAR applications, including change detection [1], [2], classification [3], [4], forest structure inversion [5], [6], terrain DEM mapping [7], [8], and earth surface deformation monitoring [9], [10], [11], [12], [13]. Among them, the phase-based applications heavily rely on the accuracy of interferometric phase or phase series estimation, which is directly related to the PolInSAR coherence matrix.

To exploit the potentials of PolInSAR coherence matrix in improving the accuracy of interferometric phase optimization, a unitary projection vector was first proposed in [14] to linearly combine data from all polarimetric channels and is optimized through the maximization of a new coherence value formed by two different projection vectors. Another optimization method with the same unitary projection vector to optimize was proposed in [15], which assumes the equality of polarimetric characteristics of two acquisitions spanned by a small baseline; in addition, a numerical radius method is applied to acquire the optimal projection vector. To ensure that the optimal projection vector is adaptive to the local characteristics in heterogenous scenes, a modified method was proposed in [8] to optimize the projection vector pixel-by-pixel. In general, these methods transform the PolInSAR coherence matrix to a new ICM through an optimized projection vector; however, as pointed out by Tabb et al. [16] and Shen et al. [17], they are often limited by the finite looking effect, i.e., the estimated coherence region is often biased due to insufficient number of looks, leading to unstable optimization results in many cases. Unlike the projection vector based methods, in [17], it was proposed to treat the interferometric coherence matrices of different polarimetric channels, i.e., the diagonal matrix elements of PolInSAR coherence matrix, as independent statistical samples and stack them up to form a TP coherence matrix, from which the optimized phase can be directly extracted. An equivalent form of the TP method

was also presented in [18], which is called trace coherence method. However, different polarimetric channels are often not independent of each other, and therefore, simply stacking the coherence matrices of different polarimetric channels together is obviously not the optimal solution and fails to fully exploit the information containing in the PolInSAR coherence matrix.

The first attempt to exploit the efficacy of multipolarimetric data in multitemporal phase series estimation is attributed to paper [9], which simply selects polarimetric channels with the highest coherence value to estimate the phase series. Later on, an ESPO method [19], [20] was further developed to find the optimal projection vector that can produce the highest average coherence value. Different from the ESPO method, in [21], the temporal coherence was employed as the objective function for projection vector optimization. But neither a maximum average coherence nor a maximum temporal coherence can guarantee the lowest root-mean-square error (RMSE) in phase series estimation. In [22], it was proposed to extract the phase series by applying a phase-linking algorithm on the TP coherence matrix. However, despite its advantages over the projection vector based methods, it is still not the optimal solution in the sense of RMSE as the information contained in the PolInSAR coherence matrix is not fully exploited. A maximum likelihood method for persistent scatters phase series optimization was proposed in [23] by assuming independence of three polarimetric channels, whereas this assumption cannot hold in most cases. Recently, a maximum likelihood estimator for multipolarimetric phase-linking (MLE-MPPL) was proposed for phase series estimation in our previous work [24], which takes the interchannel correlation into consideration and is derived within the framework of MLE under the hypothesis of CCG distribution, making it the asymptotically optimal solution under the criterion of RMSE. However, in the MLE-MPPL method, the PCM and ICM are only obtained by averaging the simple estimates over different tracks and polarimetric channels. According to the single-polarization phase linking uncertainty theory [25], [26], the accuracy of ICM exerts huge impact on phase series estimation accuracy. Analogously, inaccurate estimation of ICM and PCM in the MLE-MPPL method will degrade the phase series estimation result in the multipolarimetric case.

Therefore, to fully exploit the potential of multipolarimetric information contained in the PolInSAR coherence matrix for interferometric phase optimization and phase series estimation, an MLE of the ICM is proposed in this work. First, the PolInSAR coherence matrix is modeled as the Kronecker product of PCM and ICM. Next, the MLE of ICM under CCG distribution is analyzed and acquired through an alternate iterative optimization method. Then, in the single-baseline case, the MLE of ICM is used for interferometric phase optimization, which can achieve the best performance by fully exploiting the multipolarimetric information in the PolInSAR coherence matrix and it is the optimal solution in the sense of RMSE. In the multibaseline case, the MLE of ICM is used for phase series estimation by further employing the phase-linking algorithm. In comparison to the MLE-MPPL method, it is proved that the proposed method with the MLE of ICM can achieve better performance because it provides more accurate estimation of ICM. Moreover, the suboptimality of the TP method has also been proved by demonstrating that the TP method is only a special case of the proposed method when the PCM is an identity matrix.

The rest of this article is organized as follows. In Section II, the existing methods for multipolarimetric interferometric phase optimization and phase series estimation are briefly reviewed. The proposed MLE of ICM and its applications in interferometric phase optimization and phase series estimation are provided in Section III. Numerical results on both simulated data and real data are presented in Section IV. Finally, Section V concludes this article.

II. Existing Methods for Multipolarimetric Interferometric Phase Optimization and Phase Series Estimation

Currently, there are mainly three kinds of methods for multipolarimetric interferometric phase optimization and phase series estimation, including the projection vector based method, the TP method, and the MLE-MPPL method. The former two can be applied to both interferometric phase optimization and phase series estimation, and the MLE-MPPL method is primarily designed for phase series estimation. In this section, their basic principles are briefly reviewed.

A. PolInSAR Optimization Based on Projection Vector

In a fully polarimetric SAR acquisition, the Sinclair backscattering matrix can be vectorized by a Pauli basis scattering vector [19] as follows:

$$\mathbf{k} = \left[\frac{1}{\sqrt{2}}S_{HH+VV}, \frac{1}{\sqrt{2}}S_{HH-VV}, \sqrt{2}S_{HV}\right]^T \tag{1}$$

under the co-polar reciprocity hypothesis, where $[\cdot]^T$ denotes the transpose operator.

Given N fully polarimetric SAR single look complex (SLC) acquisitions

$$\mathbf{K} = [\mathbf{k}_1, \mathbf{k}_2, \ldots, \mathbf{k}_N]^T. \tag{2}$$

The projection vector based methods [14], [15], [19], [20] introduce a unitary projection vector $\boldsymbol{\omega}$ to compress the Pauli basis scattering vector $\mathbf{K}$ to a new vector

$$\boldsymbol{\mu} = \left[\boldsymbol{\omega}^H\mathbf{k}_1, \boldsymbol{\omega}^H\mathbf{k}_2, \ldots, \boldsymbol{\omega}^H\mathbf{k}_N\right]^T \tag{3}$$

where $(\cdot)^H$ denotes the Hermitian transpose. Then, the projection vector $\boldsymbol{\omega}$ is optimized by exploring the maximum average coherence magnitude of the newly formed coherence matrix $\mathbf{C}_{\boldsymbol{\mu}} = E(\boldsymbol{\mu}\boldsymbol{\mu}^H)$, where $E(\cdot)$ denotes expectation operator, and the optimization problem can be expressed as follows:

$$\boldsymbol{\omega}_{opt} = \arg\max_{\boldsymbol{\omega}} \frac{2}{(N-1)\,N} \sum_{i=1}^{N}\sum_{j>i}^{N} \left| \frac{\boldsymbol{\omega}^H\boldsymbol{\Omega}_{ij}\boldsymbol{\omega}}{\sqrt{\boldsymbol{\omega}^H\mathbf{T}_{ii}\boldsymbol{\omega}}\sqrt{\boldsymbol{\omega}^H\mathbf{T}_{jj}\boldsymbol{\omega}}} \right| \tag{4}$$

where $|\cdot|$ is the modulus operator, $\mathbf{T}_{ii} = E[\mathbf{k}_i\mathbf{k}_i^H]$, and $\boldsymbol{\Omega}_{ij} = E[\mathbf{k}_i\mathbf{k}_j^H], i \neq j$.

B. TP Method

The TP method [17], [22] treats the sample coherence matrices of different polarimetric channels as independent statistical samples and directly adds them up to construct the TP coherence matrix, expressed as follows:

$$\mathbf{C}_{\text{TP}} = \sum_{i=1}^{3} \hat{\mathbf{C}}_i \tag{5}$$

where $\hat{\mathbf{C}}_i$ is the sample coherence matrix of the ith polarimetric channel.

C. MLE-MPPL Method

By constructing and maximizing the multipolarimetric likelihood function, the MLE-MPPL method [24] derives the MLE of the multipolarimetric phase series $\boldsymbol{\theta}$ as follows:

$$\boldsymbol{\theta}_{\text{MLE-MPPL}} = \arg\max_{\boldsymbol{\theta}} -\boldsymbol{\Lambda}^H \left(\sum_{i=1}^{3\times 3} \text{trace}\left(\mathbf{C}_{\text{pol}}^{-1} \tilde{\mathbf{C}}_{\text{pol},i} \right) \times \left(|\mathbf{C}_{\text{coh}}|^{-1} \circ \tilde{\mathbf{C}}_{\text{coh},i} \right) \right) \boldsymbol{\Lambda} \tag{6}$$

where $\boldsymbol{\Lambda} = \exp(-j\boldsymbol{\theta})$, $\text{trace}(\cdot)$ denotes the matrix trace operator,$\circ$ is the Hadamard product, $\mathbf{C}_{\text{coh}} \in \mathbb{C}^{N\times N}$ and $\mathbf{C}_{\text{pol}} \in \mathbb{C}^{3\times 3}$ are the ICM and PCM, respectively. $\tilde{\mathbf{C}}_{\text{pol},i} \in \mathbb{C}^{3\times 3}$ and $\tilde{\mathbf{C}}_{\text{coh},i} \in \mathbb{C}^{N\times N}$ are obtained through the SKP decomposition on the sample PolInSAR coherence matrix $\hat{\mathbf{T}}$ as follows:

$$\hat{\mathbf{T}} = \sum_{i=1}^{3\times 3} \tilde{\mathbf{C}}_{\text{pol},i} \otimes \tilde{\mathbf{C}}_{\text{coh},i} \tag{7}$$

where $\otimes$ denotes the Kronecker product.

As mention earlier, the projection vector based methods are often affected by the finite looking effect in estimation of $\mathbf{T}_{ii}$ and $\boldsymbol{\Omega}_{ij}$, which can cause unstable optimization results. Besides, the maximum average coherence cannot guarantee the optimum result under the RMSE criterion. The advantages of TP method over the projection vector based methods has already validated in [17], but its independence assumption on polarimetric channels is often invalid in practice; in other words, the cross-polarization information is not exploited. The MLE-MPPL method has taken the cross-polarization information into consideration by removing all constraints on the PCM $\mathbf{C}_{\text{pol}}$ and estimating it in the process. In addition, MLE-MPPL is derived under the CCG distribution, but the PCM $\mathbf{C}_{\text{pol}}$ and ICM $\mathbf{C}_{\text{coh}}$ in MLE-MPPL are only estimated through simple average over different acquisitions and polarimetric channels, given by

$$\hat{\mathbf{C}}_{\text{pol}} = \frac{1}{N} \sum_{i=1}^{N} \mathbf{k}_i \mathbf{k}_i^H \tag{8}$$

and

$$\hat{\mathbf{C}}_{\text{coh}} = \frac{1}{3} \sum_{i=1}^{3} \hat{\mathbf{C}}_i. \tag{9}$$

Therefore, the estimations by (8) and (9) are often not accurate enough, which, according to the phase-linking uncertainty theory [25], [26], will degrade phase series estimation performance. Moreover, MLE-MPPL cannot be used directly for single-baseline interferometric phase optimization as it is primarily designed for phase series estimation. The proposed method presents the MLE of $\mathbf{C}_{\text{pol}}$ and $\mathbf{C}_{\text{coh}}$ through an alternate iterative optimization algorithm and then applies phase-linking on the MLE of $\mathbf{C}_{\text{coh}}$ for consistent phase series estimation; furthermore, the MLE of $\mathbf{C}_{\text{coh}}$ can be directly used in single baseline interferometric phase optimization.

III. MLE of ICM and its Applications on Interferometric Phase Optimization and Phase Series Estimation

In this section, an MLE of the ICM is proposed and used in both interferometric phase optimization and phase series estimation. Performance analysis is provided to demonstrate its superiority over the state-of-the-art TP method and MLE-MPPL method.

A. MLE of the ICM

Under the CCG distribution, the probability density function of N fully polarimetric SAR SLC acquisitions can be written as follows:

$$f(\mathbf{y}) = \frac{1}{\pi^N \det(\mathbf{T})} \exp\left\{ -\mathbf{K}^H \mathbf{T}^{-1} \mathbf{K} \right\} \tag{10}$$

where $\det(\cdot)$ represents the matrix determinant operator and $\mathbf{T} = E(\mathbf{K}\mathbf{K}^H)$ is the PolInSAR coherence matrix. Then, a multipolarimetric likelihood function can be constructed as follows:

$$L_{\text{pol}} = -\ln\det(\mathbf{T}) - \text{trace}\left(\mathbf{T}^{-1} \hat{\mathbf{T}} \right). \tag{11}$$

Consider the following model [5], [24] for the PolInSAR coherence matrix

$$\mathbf{T} = \mathbf{C}_{\text{pol}} \otimes \mathbf{C}_{\text{coh}}. \tag{12}$$

Substituting (7) and (12) into (11), a multipolarimetric likelihood function with respect to $\mathbf{C}_{\text{pol}}$ and $\mathbf{C}_{\text{coh}}$ can be obtained as follows:

$$L_{\text{pol}}(\mathbf{C}_{\text{pol}}, \mathbf{C}_{\text{coh}}) = -\ln\det(\mathbf{C}_{\text{pol}} \otimes \mathbf{C}_{\text{coh}}) - \sum_{i=1}^{3\times 3} \text{trace}\left((\mathbf{C}_{\text{pol}} \otimes \mathbf{C}_{\text{coh}})^{-1} \left(\tilde{\mathbf{C}}_{\text{pol},i} \otimes \tilde{\mathbf{C}}_{\text{coh},i} \right) \right). \tag{13}$$

Then, instead of further modeling $\mathbf{C}_{\text{coh}}$ as in the MLE-MPPL method, the MLE of the ICM is directly analyzed and acquired from (13) by maximizing the likelihood function $L_{\text{pol}}(\mathbf{C}_{\text{pol}}, \mathbf{C}_{\text{coh}})$.This is a bivariate function and there is no closed form solution for the MLE of $\mathbf{C}_{\text{pol}}$ and $\mathbf{C}_{\text{coh}}$. Inspired by paper [27], an alternate iterative optimization method is

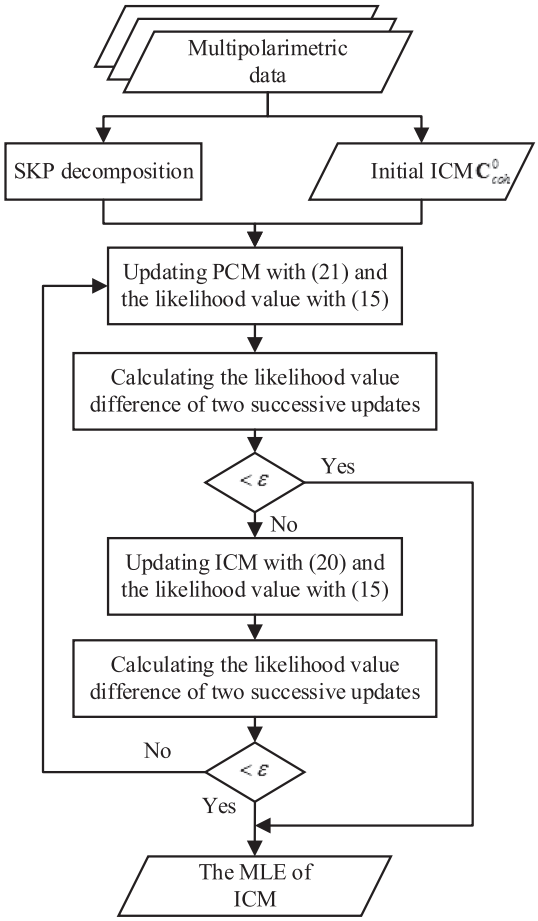

Fig. 1. Flowchart of the alternately iterative optimization for the MLE of ICM.

proposed here to find the solution. The alternate iterative relationship between $\mathbf{C}_{\text{pol}}$ and $\mathbf{C}_{\text{coh}}$ are derived as follows:

$$\mathbf{C}_{\text{coh}} = \frac{1}{3}\sum_{i=1}^{3\times 3} \tilde{\mathbf{C}}_{\text{coh},i} \text{trace}\left(\mathbf{C}_{\text{pol}}^{-1}\tilde{\mathbf{C}}_{\text{pol},i}\right) \tag{14}$$

$$\mathbf{C}_{\text{pol}} = \frac{1}{N}\sum_{i=1}^{3\times 3} \tilde{\mathbf{C}}_{\text{pol},i} \text{trace}\left(\mathbf{C}_{\text{coh}}^{-1}\tilde{\mathbf{C}}_{\text{coh},i}\right). \tag{15}$$

The detailed derivation of (14) and (15) can be found in the Appendix. Then, the MLE of ICM $\mathbf{C}_{\text{coh}}$ can be solved by an alternate iteration process, as described in Fig. 1.

First, the sample PolInSAR coherence matrix $\hat{\mathbf{T}}$ is acquired from the multipolarimetric data and decomposed into $\tilde{\mathbf{C}}_{\text{pol},i}$ and $\tilde{\mathbf{C}}_{\text{coh},i}$ through the SKP decomposition. In the meantime, an initial ICM $\mathbf{C}_{coh}^{0}$ is selected to start the iteration process, which can be roughly estimated from the multipolarimetric data as follows:

$$\mathbf{C}_{\text{coh}}^{0} = \frac{1}{3}\sum_{i=1}^{3} \hat{\mathbf{C}}_{i}. \tag{16}$$

After that, $\mathbf{C}_{\text{coh}}^{0}$ is substituted into (15) to obtain the estimated PCM $\mathbf{C}_{\text{pol}}^{1}$ as follows:

$$\mathbf{C}_{\text{pol}}^{1} = \frac{1}{N}\sum_{i=1}^{3\times 3} \tilde{\mathbf{C}}_{\text{pol},i} \text{trace}\left(\left(\mathbf{C}_{\text{coh}}^{0}\right)^{-1}\tilde{\mathbf{C}}_{\text{coh},i}\right). \tag{17}$$

Likewise, the obtained $\mathbf{C}_{\text{pol}}^{1}$ is substituted in (14) to update the ICM $\mathbf{C}_{\text{coh}}^{1}$ as follows:

$$\mathbf{C}_{\text{coh}}^{1} = \frac{1}{3}\sum_{i=1}^{3\times 3} \tilde{\mathbf{C}}_{\text{coh},i} \text{trace}\left(\left(\mathbf{C}_{\text{pol}}^{1}\right)^{-1}\tilde{\mathbf{C}}_{\text{pol},i}\right) \tag{18}$$

and $\mathbf{C}_{\text{coh}}^{1}$ is again substituted into (16) for the next iteration. At the end of each update, the newly obtained ICM and PCM are substituted into the likelihood function in (13) to calculate the corresponding likelihood value. The alternate iteration stops when the difference between the likelihood values of two successive updates is smaller than a prefixed value ε, which is set to $\varepsilon = 0.001$ here. The ICM at the end of the alternate iteration process is the final solution.

B. Application of the MLE of ICM to Interferometric Phase Optimization and Its Performance Analysis

When the multipolarimetric data are in the single-baseline configuration, the ICM is an 2×2 matrix, and the MLE can be used for interferometric phase optimization by directly extracting the optimized phase from the off-diagonal entries as follows:

$$\varphi_{\text{optimized}} = \arg\left(\left(\mathbf{C}_{\text{coh,MLE}}\right)_{1,2}\right) \tag{19}$$

where $\varphi_{\text{optimized}}$ denotes the optimized interferometric phase, $\arg(\cdot)$ denotes the argument of a complex number,$\mathbf{C}_{coh,MLE}$ the MLE of ICM, and $(\cdot)_{1,2}$ the element of a matrix at its first row and second column. If much deeper filtering effect is required, existing ICM-based [28] and interferogram-based [29] single-polarimetric phase filtering methods can be further applied to the MLE of ICM and $\varphi_{\text{optimized}}$, respectively.

To theoretically prove the effectiveness and superiority of the proposed solution for interferometric phase optimization, the relationship between the proposed method and the TP method is analyzed.

The optimized interferometric phase for the TP method is expressed as follows:

$$\varphi_{\text{optimized,TP}} = \arg\left(\left(\mathbf{C}_{\text{TP}}\right)_{1,2}\right). \tag{20}$$

According to (19) and (20), the relationship between the optimized phase by the TP method and the proposed method is determined by $\mathbf{C}_{\text{TP}}$ and $\mathbf{C}_{\text{coh,MLE}}$.

On one hand, the sample PolInSAR coherence matrix can be expressed as follows:

$$\hat{\mathbf{T}} = \begin{bmatrix} \hat{\mathbf{C}}_1 & \hat{\mathbf{C}}_{12} & \hat{\mathbf{C}}_{13} \\ \hat{\mathbf{C}}_{21} & \hat{\mathbf{C}}_2 & \hat{\mathbf{C}}_{23} \\ \hat{\mathbf{C}}_{31} & \hat{\mathbf{C}}_{32} & \hat{\mathbf{C}}_3 \end{bmatrix} \tag{21}$$

where $\hat{\mathbf{C}}_{ij}, i \neq j$ denotes the sample interchannel coherence matrix between the ith and jth polarimetric channels. In addition

to (21), $\hat{\mathbf{T}}$ can also be expressed by the SKP decomposition as in (7). Combining (7) and (21), it follows that

$$\hat{\mathbf{C}}_k = \sum_{i=1}^{3\times 3} \left(\tilde{\mathbf{C}}_{\text{pol},i}\right)_{k,k} \tilde{\mathbf{C}}_{\text{coh},i}, \quad k = 1,2,3 \tag{22}$$

where $\left(\tilde{\mathbf{C}}_{\text{pol},i}\right)_{k,k}$ is the element of $\tilde{\mathbf{C}}_{\text{pol},i}$ at the kth row and the kth column. Considering (5), it follows that

$$\mathbf{C}_{\text{TP}} = \sum_{k=1}^{3} \hat{\mathbf{C}}_k = \sum_{k=1}^{3}\sum_{i=1}^{3\times 3} \left(\tilde{\mathbf{C}}_{\text{pol},i}\right)_{k,k} \tilde{\mathbf{C}}_{\text{coh},i}. \tag{23}$$

Changing the order of the two summations on the right side of (23), we have

$$\mathbf{C}_{\text{TP}} = \sum_{i=1}^{3\times 3}\sum_{k=1}^{3} \left(\tilde{\mathbf{C}}_{\text{pol},i}\right)_{k,k} \tilde{\mathbf{C}}_{\text{coh},i} = \sum_{i=1}^{3\times 3} \tilde{\mathbf{C}}_{\text{coh},i} \text{trace}\left(\tilde{\mathbf{C}}_{\text{pol},i}\right). \tag{24}$$

On the other hand, considering the iterative relationship between the ICM and PCM in (14), the MLE of ICM can be expressed as follows:

$$\mathbf{C}_{\text{coh,MLE}} = \frac{1}{3}\sum_{i=1}^{3\times 3} \tilde{\mathbf{C}}_{\text{coh},i} \text{trace}\left(\mathbf{C}_{\text{pol,MLE}}^{-1} \tilde{\mathbf{C}}_{\text{pol},i}\right) \tag{25}$$

where $\mathbf{C}_{\text{pol,MLE}}$ is the MLE of PCM. Replacing the $\mathbf{C}_{\text{pol.MLE}}$ term in (25) with an identity matrix, the MLE of ICM becomes

$$\mathbf{C}_{\text{coh,MLE}} = \frac{1}{3}\sum_{i=1}^{3\times 3} \tilde{\mathbf{C}}_{\text{coh},i} \text{trace}\left(\tilde{\mathbf{C}}_{\text{pol},i}\right) \tag{26}$$

where the constant scaling factor of $1/3$ can be ignored as it does not affect the optimized interferometric phase. It can be found from (24) and (26) that the TP coherence matrix is equivalent to the MLE of the ICM when the PCM is an identity matrix, indicating that the TP method is a special case of the proposed method.

However, the PCM is often not an identity matrix, and the TP method only uses the information of the diagonal elements in (21) by assuming that the PCM is an identity matrix, whereas the MLE of ICM has integrated all the information in $\hat{\mathbf{T}}$ by considering the MLE of the PCM, rather than an identity matrix. Hence, a better performance on interferometric phase optimization can be expected by the proposed method.

C. Application of the MLE of ICM to Phase Series Estimation and Its Performance Analysis

When dealing with multitemporal multipolarimetric data, the MLE of ICM can be used for phase series estimation through phase-linking algorithms [30], [31], [32], [33]. The EMI phase-linking algorithm [33] is employed here to retrieve the phase series from the MLE of ICM, which can be expressed as follows:

$$\boldsymbol{\theta}_{\text{ICM}} = \arg\max_{\boldsymbol{\theta}} -\boldsymbol{\Lambda}^H \left(\left|\mathbf{C}_{\text{coh.MLE}}\right|^{-1} \circ \mathbf{C}_{\text{coh.MLE}}\right) \boldsymbol{\Lambda} \tag{27}$$

where $\boldsymbol{\theta}_{\text{ICM}}$ is the phase series to be retrieved. Similar to (6), the optimization problem in (27) can be solved using EVD.

To theoretically prove the effectiveness and superiority of the MLE of ICM on phase series estimation, its solution for phase series estimation is compared to that of the state-of-the-art MLE-MPPL method and TP method.

Replacing the $\mathbf{C}_{\text{coh.MLE}}$ term on the right-hand side of Hadamard product in (27) with the expression in (25), it follows that

$$\boldsymbol{\theta}_{\text{ICM}} = \arg\max_{\boldsymbol{\theta}} -\frac{1}{3}\boldsymbol{\Lambda}^H \left(\left|\mathbf{C}_{\text{coh.MLE}}\right|^{-1} \circ \left(\sum_{i=1}^{3\times 3} \tilde{\mathbf{C}}_{\text{coh},i} \text{trace}\left(\mathbf{C}_{\text{pol,MLE}}^{-1} \tilde{\mathbf{C}}_{\text{pol},i}\right)\right)\right) \boldsymbol{\Lambda}. \tag{28}$$

Ignoring the constant scaling factor $1/3$ and moving the $\left|\mathbf{C}_{\text{coh.MLE}}\right|^{-1}$ term into the summation, (28) can be further transformed into

$$\boldsymbol{\theta}_{\text{ICM}} = \arg\max_{\boldsymbol{\theta}} -\boldsymbol{\Lambda}^H \left(\sum_{i=1}^{3\times 3} \text{trace}\left(\mathbf{C}_{\text{pol,MLE}}^{-1} \tilde{\mathbf{C}}_{\text{pol},i}\right) \times \left(\left|\mathbf{C}_{\text{coh,MLE}}\right|^{-1} \circ \tilde{\mathbf{C}}_{\text{coh},i}\right)\right) \boldsymbol{\Lambda}. \tag{29}$$

Compared to (6), it can be found that the phase series estimation solution using the MLE of ICM shares a similar form with the MLE-MPPL method. However, it provides more accurate estimations for the PCM and ICM, i.e., $\mathbf{C}_{\text{coh,MLE}}$ and $\mathbf{C}_{\text{coh,MLE}}$, than the MLE-MPPL method. Hence, according to phase-linking uncertainty theory [25], [26], the proposed method with the MLE of ICM can achieve more accurate phase series estimation than the MLE-MPPL method.

The solutions for phase series estimation by the TP method and the proposed method are obtained by employing the phase linking algorithm on $\mathbf{C}_{\text{TP}}$ and $\mathbf{C}_{\text{coh,MLE}}$, which indicates that their estimation performance is completely determined by these two factors. Therefore, the proposed method can achieve better performance than the TP method as $\mathbf{C}_{\text{TP}}$ is only a special case of $\mathbf{C}_{\text{coh,MLE}}$ when the PCM is an identity matrix, which has already been proved earlier.

IV. Numerical Results

In this section, simulation results and experiments on real data are presented to demonstrate the effectiveness of the proposed method, where the proposed alternate iterative optimization method for the MLE of ICM is verified by its convergence performance and estimation accuracy, and the performance of the proposed MLE of ICM on interferometric phase optimization and phase series estimation is assessed by comparing with the existing methods. In real data experiments, fully polarimetric airborne SAR data and dual polarimetric spaceborne SAR data are employed for interferometric phase optimization and phase series estimation, respectively.

A. Simulation Results

The multipolarimetric data are simulated using the Monte Carlo method in [34] with a given PolInSAR coherence matrix, which is modeled as the Kronecker product of $\mathbf{C}_{\text{pol}}$ and $\mathbf{C}_{\text{coh}}$as

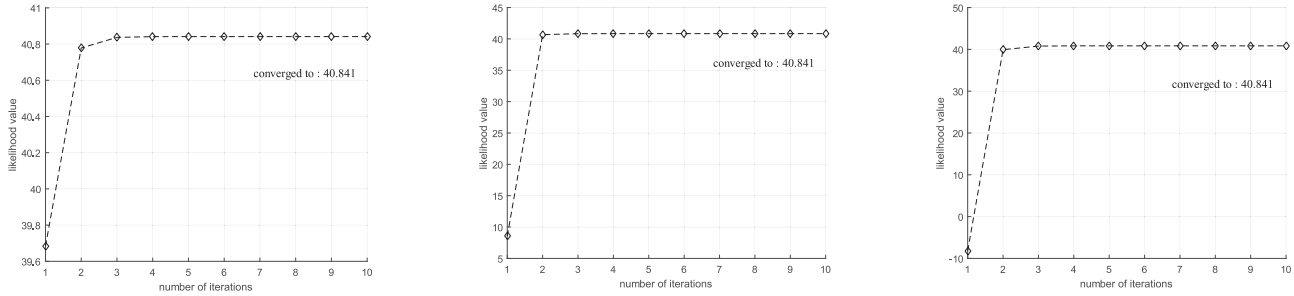

(a) (b) (c)

Fig. 2. Convergence curves by three different initial ICMs. (a) Initial ICM from (16). (b) Identity matrix. (c) Random matrix.

in (12). Therefore, the modeling of PolInSAR coherence matrix breaks down to the modeling of $\mathbf{C}_{\text{pol}}$ and $\mathbf{C}_{\text{coh}}$.

The extended Bragg scattering model [3] is considered for the modeling of $\mathbf{C}_{\text{pol}}$, as in [24].

$\mathbf{C}_{\text{coh}}$ can be modeled by its phase and magnitude terms as follows:

$$\mathbf{C}_{\text{coh}} = \mathbf{\Theta}^H \mathbf{\Gamma} \mathbf{\Theta} \tag{30}$$

where $\mathbf{\Theta} = \text{diag}[\exp(-j\boldsymbol{\theta})]$, $\boldsymbol{\theta} = [\theta_1, \theta_2, \ldots, \theta_N]^T$ denotes the phase term, and $\mathbf{\Gamma} \in \mathbb{R}^{N\times N}$ is the magnitude term. The phase term $\boldsymbol{\theta}$ is generated by considering a constant deformation velocity of 1 cm/year. A general temporal decorrelation model is considered for $\mathbf{\Gamma}$ [33], which is

$$(\mathbf{\Gamma})_{ij} = (\gamma_0 - \gamma_\infty)\exp(-\delta t_{ij}/\tau) + \gamma_\infty \tag{31}$$

where $(\mathbf{\Gamma})_{ij}$ is the element of $\mathbf{\Gamma}$ at the ith row and jth column, γ_0 and γ_∞ are the initial coherence and the long-term coherence values, respectively, δt_{ij} is the temporal baseline between the ith and jth acquisitions, and τ indicates the extent to which the coherence decreases with the temporal baseline. Here γ_0 and γ_∞ are set to 0.6 and 0.2, respectively, τ is set to 50 days, and the sampling interval for temporal baseline $\tau_0$is 6 days. Since a single phase center is assumed in this paper, volume decorrelation is not considered, and the atmospheric phase is also ignored here to ensure stationarity of simulated CCG data, as in [33].

Three different groups of phase series are generated. Without loss of generality, the first element of each phase series is set to zero. The first group of phase series $\boldsymbol{\theta}_1$ is 1-D and generated by applying a constant deformation velocity 1 cm/year, and a total of 20 fully polarimetric SLC images with 6 days temporal sampling interval are simulated with 100 independent samples for verifying the alternate iterative optimization and phase series estimation; the second one $\boldsymbol{\theta}_2$ is 2-D with only two SLC images and the interferogram between the two SLC images is generated by mapping a realistic DEM provided by NASA SRTM mission into the SAR coordinates. The temporal baseline between the two SLC images is 30 days for interferometric phase optimization; the third one $\boldsymbol{\theta}_3$ is also 2-D, and the temporal and spatial patterns of the phase series are generated by applying a constant deformation velocity and MATLAB's peaks function, respectively. Like $\boldsymbol{\theta}_1$, a total of 20 fully polarimetric SLC images with 6 days temporal sampling interval are simulated for phase series estimation.

TABLE I
AVERAGE NUMBER OF ITERATIONS WITH THREE DIFFERENT INITIAL MATRICES

The one in (16)	Identity matrix	Random matrix
5.000	5.488	7.161

1) Convergence Performance and Estimation Accuracy of the Alternate Iterative Optimization Method: Using the simulated multipolarimetric data generated by $\boldsymbol{\theta}_1$, the sample PolInSAR coherence matrix $\hat{\mathbf{T}}$ can be acquired and then decomposed into $\tilde{\mathbf{C}}_{\text{pol},i}$ and $\tilde{\mathbf{C}}_{\text{coh},i}$ through the SKP decomposition, while the initial ICM is obtained using (16). In addition, an identity matrix and a random matrix are also employed as the initial ICM to start the alternate iteration. The corresponding convergence curves using three initial ICMs are plotted in Fig. 2(a)–(c), respectively. Moreover, to show the convergence speed, 1000 independent simulations are conducted and the average number of iterations with the three initial matrices are calculated and listed in Table I. It can be seen from Fig. 2 that the proposed alternate iteration method converges to the same value under all three different initializations within a few iterations, even with the random initial matrix. Among the three initial matrices, the one provided by (16) takes the least number of iterations to converge, on average 5.000 iterations, and the random initial matrix takes the most number of iterations to converge, which is 7.161 iterations on average, as shown in Table I. In addition, a correlation coefficient ρ is proposed to evaluate the estimation accuracy of the estimated PCM and ICM, which is defined as follows:

$$\begin{cases} \rho_{\text{PCM}} = \dfrac{\left|\sum_{i=1}^{3}\sum_{j=1}^{3}\left(\mathbf{C}_{\text{pol}}\circ\hat{\mathbf{C}}_{\text{pol}}^*\right)_{ij}\right|}{\|\mathbf{C}_{\text{pol}}\|_F\left\|\hat{\mathbf{C}}_{\text{pol}}^*\right\|_F} \\ \rho_{\text{ICM}} = \dfrac{\left|\sum_{i=1}^{N}\sum_{j=1}^{N}\left(\mathbf{C}_{\text{coh}}\circ\hat{\mathbf{C}}_{\text{coh}}^*\right)_{ij}\right|}{\|\mathbf{C}_{\text{coh}}\|_F\left\|\hat{\mathbf{C}}_{\text{coh}}^*\right\|_F} \end{cases} \tag{32}$$

where $\|\cdot\|_F$ denotes the Frobenius norm, $(\cdot)^*$ represents the complex conjugate, and $\hat{\mathbf{C}}_{\text{pol}}$ and $\hat{\mathbf{C}}_{\text{coh}}$ are the estimated PCM and ICM, respectively. According to (32), ρ_{PCM} and ρ_{ICM} reflect the similarity between the estimated PCM, ICM and their corresponding true values, respectively. The closer ρ_{PCM} and ρ_{ICM} are to one, the more accurate the estimated PCM and ICM. About 1000 independent simulation runs are conducted on the multipolarimetric data generated using the first group of phase series $\boldsymbol{\theta}_1$. The histograms of ρ_{PCM} using the proposed

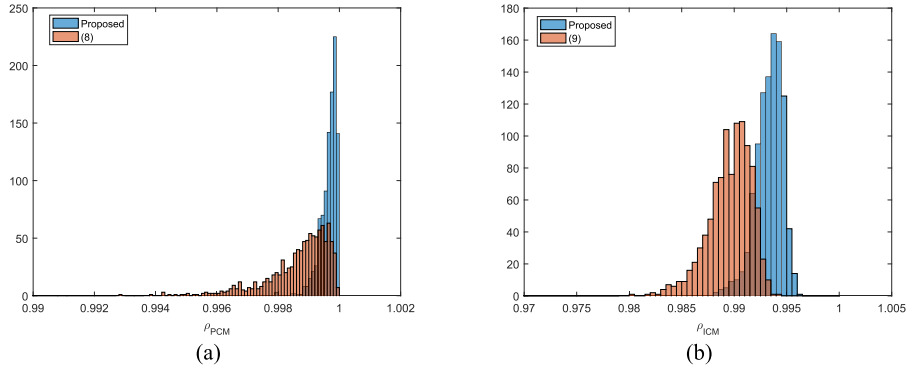

Fig. 3. Histograms of ρ_{PCM} and ρ_{ICM} by two methods. (a) Histograms of the ρ_{PCM}. (b) Histograms of the ρ_{ICM}.

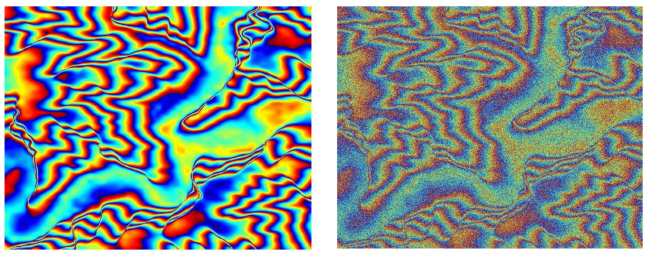

Fig. 4. True interferogram and the single polarimetric noisy interferogram formed by the two simulated SLC images. (a) True interferogram. (b) Single polarimetric noisy interferogram.

alternate iteration method and (8) are shown in Fig. 3(a), and those of ρ_{ICM} using the proposed alternate iteration method and (9) are shown in Fig. 3(b). It can be observed from Fig. 3 that the histograms of ρ_{PCM} and ρ_{ICM} by the proposed alternate iteration method are more concentrated around one than those by (8) and (9), indicating the effectiveness and superiority of the proposed alternate iteration method.

2) Performance on Interferometric Phase Optimization: For interferometric phase optimization, the second group of phase series $\boldsymbol{\theta}_2$ with only two SLC images are employed to simulate multipolarimetric data and the dimension of each SLC image is 1000×1000. Three other methods, including single polarimetric boxcar method, the numerical radius (NR) method [15] and the TP method [17], are also applied and compared with the proposed method. A 7×7 window is selected to estimate the PolInSAR coherence matrix. The true interferogram and the single polarimetric noisy interferogram formed by the simulated SLC images are shown in Fig. 4(a) and (b), respectively. The optimized interferograms by four methods are shown in Fig. 5 and their corresponding histograms for estimation error are shown in Fig. 6.

It can be seen from Fig. 6 that the estimation error by the NR method is the largest among three multipolarimetric methods, with the RMSE of 0.3324 rad, which is even worse than that of the single polarimetric method, indicating the instability of the NR method. A similar result has also been reported in [17]. Compared to the TP method, the result by the proposed method looks thinner and more concentrated around zero, with the lowest RMSE of 0.2510 rad among all four methods. Hence, the proposed MLE of the ICM has achieved the best performance for interferometric phase optimization.

3) Performance on Phase Series Estimation: For phase series estimation, both the 1-D phase series $\boldsymbol{\theta}_1$ from first group and the 2-D phase series $\boldsymbol{\theta}_3$ from the third group are employed to simulate the multipolarimetric data. The projection vector based ESPO method [20], the TP method [22], the MLE-MPPL method [24], and the proposed method are applied and their phase series estimation performance compared. In the ESPO method, the searching step size for the parameter group $(\alpha, \beta, \delta, \varphi)$ is set to $(5^\circ, 5^\circ, 5^\circ, 5^\circ)$. To retrieve the phase series, the EMI phase linking algorithm [33] is used in the ESPO, TP and proposed methods.

For the 1-D data, Fig. 7 shows the RMSE curves of four different methods with 1000 independent runs. In addition, the Cramer-Rao lower bound (CRLB) for multipolarimetric phase series estimation [24] is also plotted in Fig. 7. It can be observed from Fig. 7 that the RMSE curve of the MLE-MPPL method and the proposed method is much lower than those of ESPO and TP, while the RMSE of the proposed method is the closest to the CRLB, achieving the very best performance in phase series estimation.

For the 2-D data, the interferograms constructed by estimated phase series of four methods are shown in Fig. 8, using the first and ith images, where $i = 4, 8, 12, 16, 20$, respectively. The average RMSEs of the four methods are calculated and listed in Table II. To further demonstrate the detail preservation ability of the proposed method, a typical area with dense fringe is selected (see the black rectangular area in Fig. 8) and its enlarged view is shown in Fig. 9. It can be seen that the proposed method has achieved the best performance in recovering the fringe pattern. Moreover, Table II shows that the proposed method presents the lowest average RMSE among the four methods.

B. Real Data Experiments

To further verify the effectiveness of the proposed method, a set of L-band airborne fully polarimetric data and C-band spaceborne dual polarimetric data are employed for interferometric phase optimization and phase series estimation, respectively.

1) Interferometric Phase Optimization on E-SAR Data: The airborne data are provided by European Space Agency through

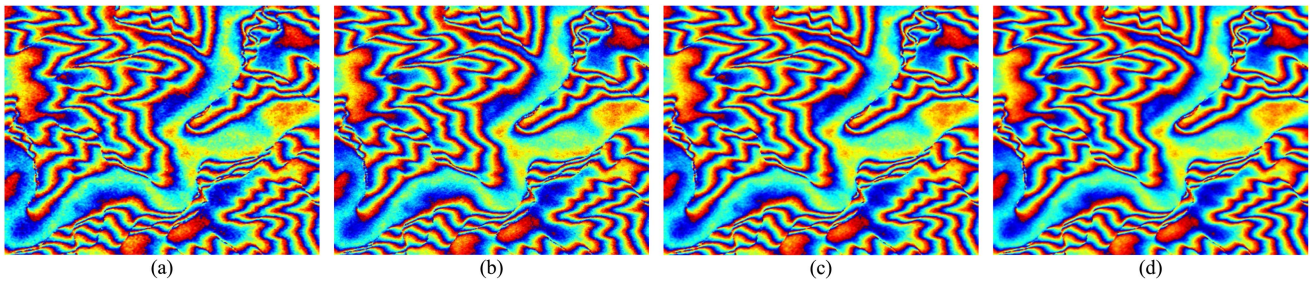

Fig. 5. Optimized interferograms by four methods. (a) Single polarimetric boxcar. (b) NR. (c) TP. (d) Proposed.

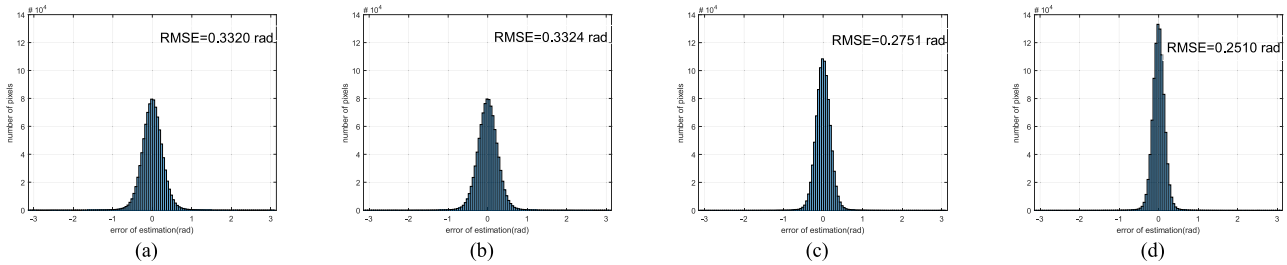

Fig. 6. Histograms of estimation error by four methods. (a) Single polarimetric boxcar. (b) NR. (c) TP. (d) Proposed.

TABLE II
AVERAGE RMSES OF FOUR METHODS

ESPO	TP	MLE-MPPL	Proposed
0.2468 rad	0.2024 rad	0.1723 rad	0.1547 rad

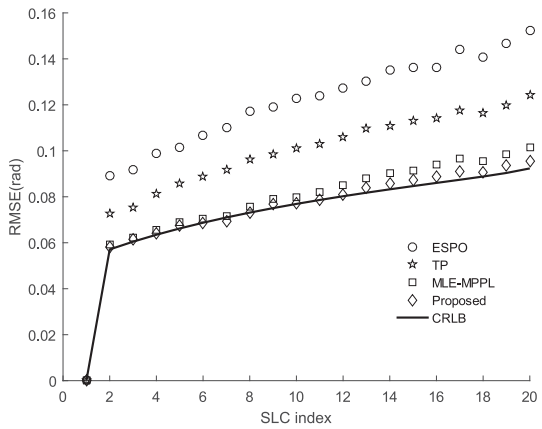

Fig. 7. RMSE curves of four different methods.

the E-SAR BioSAR2008 campaign carried out in October 2008, which is primarily designed for tomographic inversion of forest structure and biomass retrieval. The test site is located at the Krycklan River catchment, Sweden. BioSAR2008 campaign provides six tracks of fully polarimetric SAR SLC data, from which the two tracks with the longest spatial baseline are selected in this experiment. Detailed parameters about the selected data are listed in Table III. The optical image from Google Earth and the PauliRGB SAR intensity image of the investigated scene are shown in Fig. 10(a) and (b), respectively. The single look interferogram constructed by the original VV polarimetric channel is shown in Fig. 10(c). The single polarimetric boxcar method, the NR method, and the TP method are also applied and compared with the proposed method. The windows size to estimate the PolInSAR coherence matrix is 7×7 and the optimized interferograms by these four methods are shown in Fig. 11. To quantitatively evaluate the performance of these methods, the pseudo coherence ρ_ϕ [35] and number of residue points [36] are introduced. The pseudo coherence represents the spatial variance in a local window and thereby can reflect the smoothness and stability of an interferogram, and higher ρ_ϕ indicates higher phase quality. The number of residue points is also a common metric as it can reflect the difficulty of subsequent phase unwrapping operation, which is a necessary step in many applications. Less residue points indicate higher phase quality and can therefore lead to less phase unwrapping errors.

The distributions of the pseudo coherence value of the interferograms by four methods are plotted in Fig. 12(a). To highlight the differences of these methods at the high pseudo coherence end, the blue rectangular area in Fig. 12(a) is selected and its enlarged view is given in Fig. 12(b). The average pseudo coherence value and the number of residue points are listed in Table IV. In addition, the pixels with pseudo coherence $\rho_\phi > 0.7$ are defined as high quality ones and their numbers by four different methods are listed in Table IV.

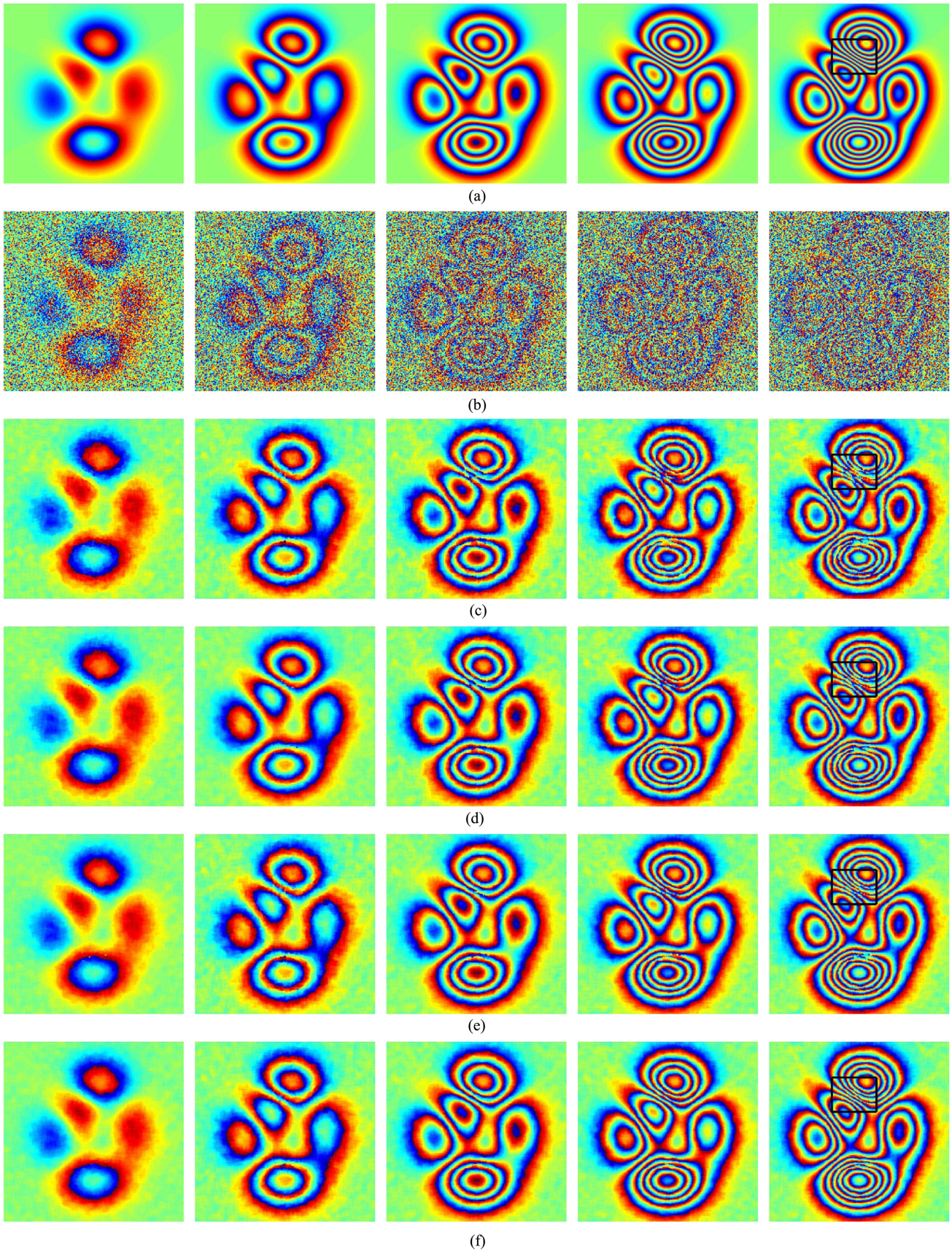

Fig. 8. Interferograms constructed by the first and $i$thimages, $i = 4, 8, 12, 16, 20$, respectively, (left to right) by each method. (a) Reference. (b) Original single polarimetric channel. (c) ESPO. (d) TP. (e) MLE-MPPL. (f) Proposed.

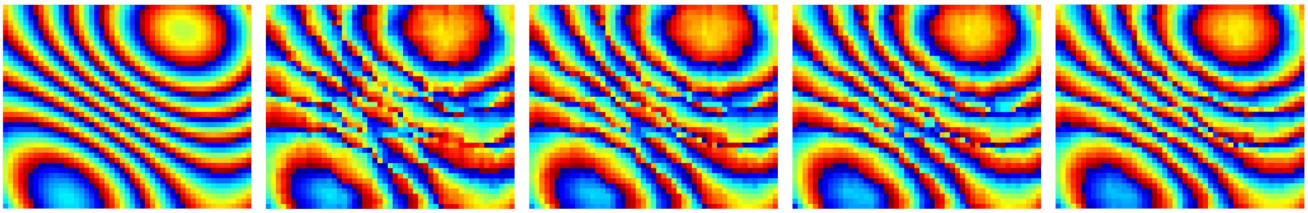

Fig. 9. Enlarged views of the black rectangular areas in Fig. 8 by different methods. (a) Reference. (b) ESPO. (c) TP. (d) MLE-MPPL. (e) Proposed.

TABLE III
DETAILED PARAMETERS ABOUT THE SELECTED E-SAR DATA

Master image acquisition time (UTC)	Slave image acquisition time (UTC)	Baseline (m)	Range resolution (m)	Azimuth resolution (m)	Frequency (GHz)
15, October 2008 09:56:42	October 15, 2008 11:20:54	30	2.12	1.20	1.3

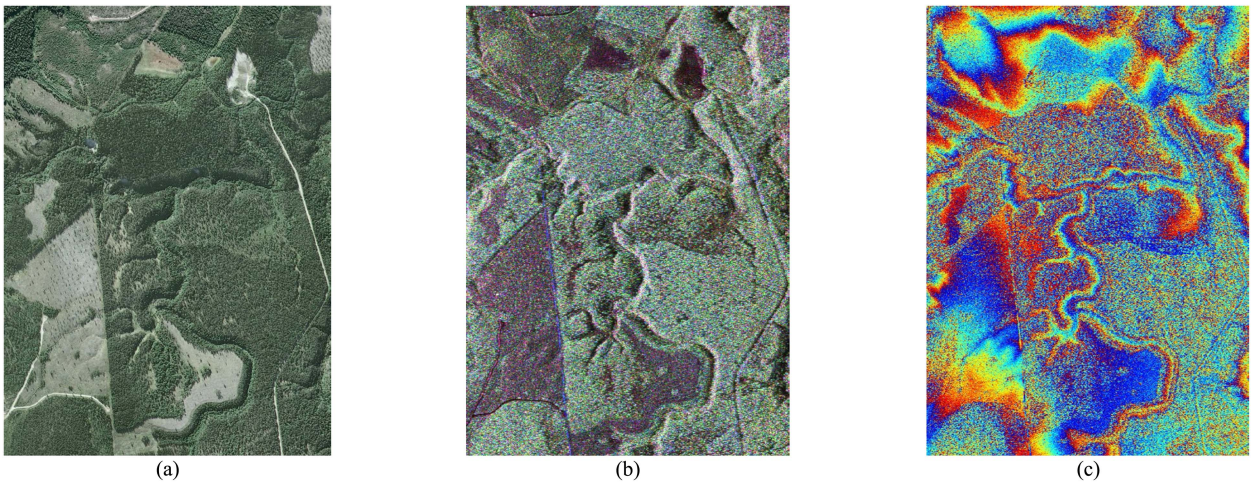

Fig. 10. Optical, SAR intensity, and interferogram images of the investigated scene. (a) Google Earth optical image. (b) PauliRGB SAR intensity image. (c) Single look interferogram from VV channel.

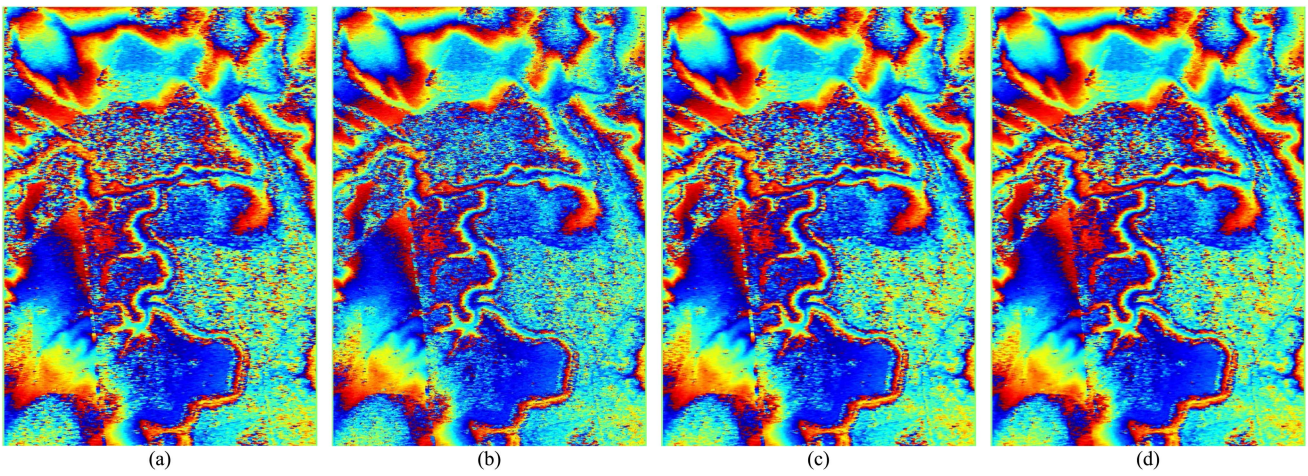

Fig. 11. Optimized interferograms by four methods. (a) Single pol. (b) NR. (c) TP. (d) Proposed.

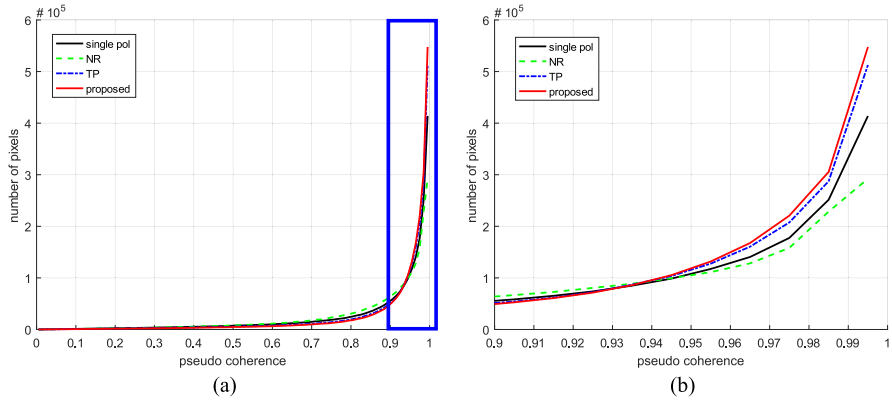

Fig. 12. Distributions of the pseudo coherence value by four methods. (a) Original distributions of the pseudo coherence. (b) Enlarged view of the blue rectangular area in (a).

TABLE IV
INTERFEROMETRIC PHASE OPTIMIZATION PERFORMANCE EVALUATION OF FOUR METHODS

Method	Average pseudo coherence	Number of residue points	Number of high quality pixels ($\times 10^6$)
Single pol	0.8617	11 184	2.037
NR	0.8468	16 791	2.003
TP	0.8890	7409	2.134
Proposed	0.8993	6961	2.170

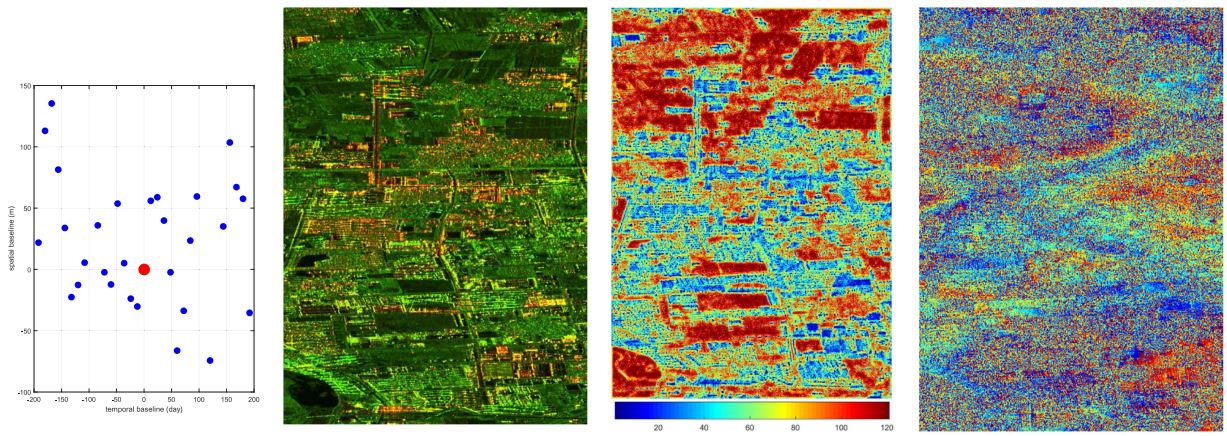

Fig. 13. Illustration of the investigated scene and corresponding dataset. (a) Spatial-temporal baseline distribution of the dataset. (b) PauliRGB image of the investigated scene (Red: $|VV|$,Green: $|VH|$, Blue: 0). (c) Map of SHPs number. (d) Single look VV interferogram constructed by the first and 30th images.

From Table IV and Fig. 12, it can be observed that the proposed method has the highest average pseudo coherence, largest number of high quality pixels, and lowest number of residue points, and its pseudo coherence distribution is more concentrated around one than the other three, indicating the best performance in interferometric phase optimization.

2) Phase Series Estimation on Sentinel-1A Data: The space-borne dual polarimetric data are acquired by ESA's C-band Sentinel-1A satellite with VV-VH polarization. A total of 30 VV-VH SAR SLC images of northern China area acquired from December 10, 2017 to December 29, 2018 are selected. The average time interval between two adjacent acquisitions is about 12 days and the spatial-temporal baseline distribution of the dataset is shown in Fig. 13(a), where the common master image is acquired on June 20, 2018. The investigated scene is situated in Yanjiao Town, Hebei Province. The temporally averaged PauliRGB SAR intensity image of the investigated scene is shown in Fig. 13(b).

Prior to phase series estimation, all other 29 images are coregistered to the common master image using the enhanced spectral diversity method [37]. The flat earth phase and topographic phase in each SLC image are all removed

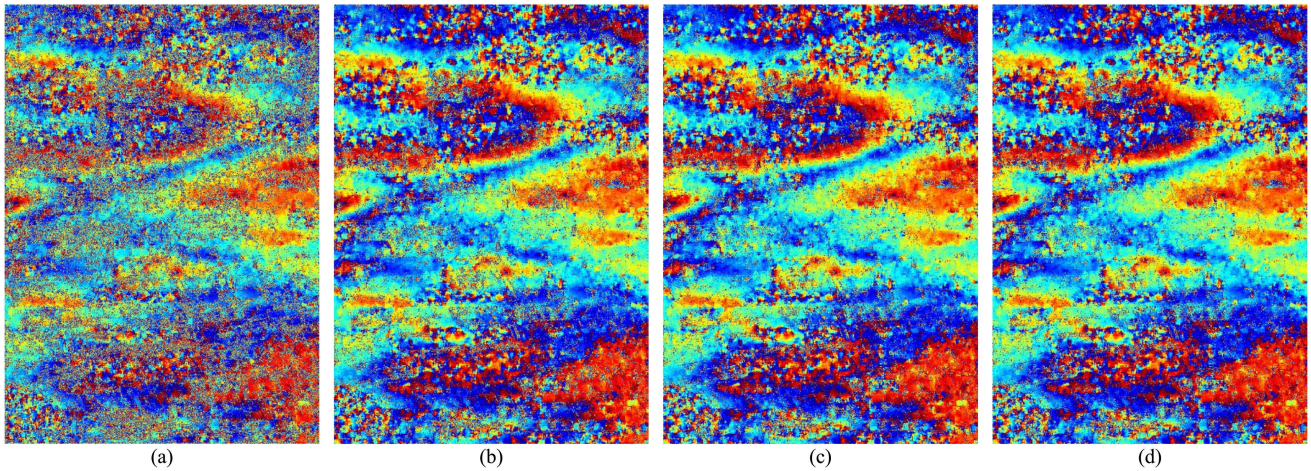

Fig. 14. Interferograms constructed by the first and 30th images of each method. (a) ESPO. (b) TP. (c) MLE-MPPL. (d) Proposed.

using the DEM provided by NASA SRTM mission. And the Kolmogorov–Smirnov (KS) test [30] with significance level $\alpha = 0.01$ and a 15×15 test window is applied to identify statistical homogeneous pixels (SHPs) for the estimation of PolInSAR coherence matrix. The KS test is applied on both polarimetric channels, and pixels that are identified as SHPs in both channels are used for PolInSAR coherence estimation. Fig. 13(c) shows the map of SHPs number of each pixel. The original single look interferogram constructed by the first and 30th images of the VV channel is shown in Fig. 13(d).

The four methods including ESPO, TP, MLE-MPPL, and the proposed one are applied for phase series estimation. To demonstrate their phase restoration capabilities, the interferometric phase of the largest temporal baseline is shown as a representative, i.e., the interferometric phase of the first and the 30th SLC images. Therefore, the interferogram in Fig. 13(d) is constructed by the first and the 30th SLC images with VV polarization. Similarly, the interferograms in Fig. 14 are generated from the estimated phase series of the four methods by subtracting the first element from the 30th element. By comparing the restored phase from the largest temporal decorrelation interferometric pair, their performance is evaluated. In addition to pseudo coherence, the number of residue points and the number of high quality pixels, the Pol-detR proposed in [24] is also introduced to quantitatively assess the performance, and a lower average Pol-detR indicates a lower average RMSE in phase series estimation. Pseudo coherence distributions of the interferograms are shown in Fig. 15, and the number of residue points, the number of high quality pixels, the average Pol-detR value, and the average pseudo coherence value by the four methods are listed in Table V.

It can be observed from Fig. 15 and Table V that the pseudo coherence by the proposed method is more concentrated around one and presents a higher average value than the other three methods. In addition, the proposed method has the lowest number residue points and the highest number of high quality pixels. These statistics indicate that the proposed method can produce the best quality interferogram among four methods. Moreover, the average Pol-detR value of the proposed method

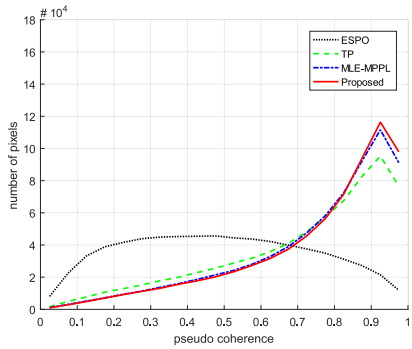

Fig. 15. Distributions of the pseudo coherence value by four methods.

TABLE V
PHASE SERIES ESTIMATION PERFORMANCE EVALUATION OF FOUR METHODS

Method	Average Pol-detR value	Average pseudo coherence	Number of residue points	Number of high quality pixels	Running time (hour)
ESPO	26.40	0.4886	115 247	164 132	43.91
TP	24.39	0.7092	47 140	427 403	3.183
MLE-MPPL	23.95	0.7441	35 782	473 079	9.252
Proposed	23.82	0.7511	34 134	481 686	10.38

is also the lowest, which implies that it can achieve the minimum average RMSE in phase series estimation. Despite that the improvement of the proposed method with respect to the MLE-MPPL method is not such significant, it can be applied to both single-baseline and multibaseline or multitemporal scenarios, whereas the MLE-MPPL method is primarily designed for multitemporal and multibaseline scenarios and therefore not applicable to the single-baseline phase optimization. Moreover, with the explicit ICM, many other phase linking algorithms [38], [39] can be adopted to adapt to different scenarios, rather than just the EMI algorithm [33] in the MLE-MPPL method.

In terms of computational load, the proposed method requires an additional alternate iteration process compared to the MLE-MPPL method. Nevertheless, the iteration converges after only a few iterations (typically 5), which has been demonstrated

in the simulation results (see Table I). Therefore, the additional computational load incurred compared to the MLE-MPPL method is small. To quantitatively evaluate the computational burden, the program running time of the four methods on the sentinel-1A dataset is listed in Table V. It can be found that the program running time of ESPO is the largest due to its exhaustive searching process in the solution space; TP is the fastest as it simply adds up the coherence matrices of different polarimetric channels; MLE-MPPL and the proposed method are slower than TP as they both involve SKP decomposition. In addition, the proposed method is slightly slower than MLE-MPPL since it demands additional alternate iteration.

V. Conclusion and Discussions

In this work, an MLE method for the ICM has been proposed and applied for both interferometric phase optimization and consistent phase series estimation. By modeling the PolInSAR coherence matrix as the Kronecker product of PCM and ICM, the estimation under the CCG distribution assumption is obtained through an alternate iterative optimization process. Its superiority on interferometric phase optimization and phase series estimation over the state-of-the-art TP method and the MLE-MPPL method has been proved theoretically, and also demonstrated by simulation results and experiments based on real data. Potential estimate errors can happen when the sample polarimetric ICM is estimated using a rectangular spatial window in heterogeneous contexts, which can be greatly alleviated by performing polarimetric homogeneous pixel selection. The limitation of the proposed method lies in its computational efficiency and single phase center assumption, which makes it less suitable for real-time processing or dense forest scenarios. Therefore, future work will focus on polarimetric homogeneous pixel selection and extending single phase center model to double or even multiple phase center model.

Appendix

Detailed derivation of the alternate iteration relationship between $\mathbf{C}_{\text{pol}}$ and $\mathbf{C}_{\text{coh}}$ is derived in this Appendix.

Invoking the determinant, inverse, trace, and mix-product properties of Kronecker product (see in [24]), (13) can be transformed into

$$\begin{aligned} &L_{\text{pol}}\left(\mathbf{C}_{\text{pol}},\mathbf{C}_{\text{coh}}\right) \\ &= -\sum_{i=1}^{3\times 3}\text{trace}\left(\mathbf{C}_{\text{pol}}^{-1}\tilde{\mathbf{C}}_{\text{pol},i}\right)\text{trace}\left(\mathbf{C}_{\text{coh}}^{-1}\tilde{\mathbf{C}}_{\text{coh},i}\right) \\ &\quad -3\ln\det\left(\mathbf{C}_{\text{coh}}\right)-N\ln\det\left(\mathbf{C}_{\text{pol}}\right). \end{aligned} \tag{33}$$

Consider the partial derivatives of $L_{\text{pol}}(\mathbf{C}_{\text{pol}},\mathbf{C}_{\text{coh}})$ with respect to $\mathbf{C}_{\text{pol}}$ and $\mathbf{C}_{\text{coh}}$, which are

$$\begin{aligned} \frac{\partial L_{\text{pol}}\left(\mathbf{C}_{\text{pol}},\mathbf{C}_{\text{coh}}\right)}{\partial \mathbf{C}_{\text{pol}}} &= \mathbf{C}_{\text{pol}}^{-1}\left(\sum_{i=1}^{3\times 3}\tilde{\mathbf{C}}_{\text{pol},i}\text{trace}\left(\mathbf{C}_{\text{coh}}^{-1}\tilde{\mathbf{C}}_{\text{coh},i}\right)\right) \\ &\quad \mathbf{C}_{\text{pol}}^{-1}-N\mathbf{C}_{\text{pol}}^{-1} \end{aligned} \tag{34}$$

and

$$\begin{aligned} \frac{\partial L_{\text{pol}}\left(\mathbf{C}_{\text{pol}},\mathbf{C}_{\text{coh}}\right)}{\partial \mathbf{C}_{\text{coh}}} &= \mathbf{C}_{\text{coh}}^{-1}\left(\sum_{i=1}^{3\times 3}\tilde{\mathbf{C}}_{\text{coh},i}\text{trace}\left(\mathbf{C}_{\text{pol}}^{-1}\tilde{\mathbf{C}}_{\text{pol},i}\right)\right) \\ &\quad \mathbf{C}_{\text{coh}}^{-1}-3\mathbf{C}_{\text{coh}}^{-1} \end{aligned} \tag{35}$$

respectively. The necessary condition for $\mathbf{C}_{\text{pol}}$ and $\mathbf{C}_{\text{coh}}$ to reach the maximum value is

$$\mathbf{C}_{\text{pol}}^{-1}\left(\sum_{i=1}^{3\times 3}\tilde{\mathbf{C}}_{\text{pol},i}\text{trace}\left(\mathbf{C}_{\text{coh}}^{-1}\tilde{\mathbf{C}}_{\text{coh},i}\right)\right)\mathbf{C}_{\text{pol}}^{-1}-N\mathbf{C}_{\text{pol}}^{-1}=\mathbf{0} \tag{36}$$

and

$$\mathbf{C}_{\text{coh}}^{-1}\left(\sum_{i=1}^{3\times 3}\tilde{\mathbf{C}}_{\text{coh},i}\text{trace}\left(\mathbf{C}_{\text{pol}}^{-1}\tilde{\mathbf{C}}_{\text{pol},i}\right)\right)\mathbf{C}_{\text{coh}}^{-1}-3\mathbf{C}_{\text{coh}}^{-1}=\mathbf{0} \tag{37}$$

respectively. According to (36) and (37), the following alternate iteration relationship between $\mathbf{C}_{\text{pol}}$ and $\mathbf{C}_{\text{coh}}$ can be derived:

$$\mathbf{C}_{\text{coh}}=\frac{1}{3}\sum_{i=1}^{3\times 3}\tilde{\mathbf{C}}_{\text{coh},i}\text{trace}\left(\mathbf{C}_{\text{pol}}^{-1}\tilde{\mathbf{C}}_{\text{pol},i}\right) \tag{38}$$

$$\mathbf{C}_{\text{pol}}=\frac{1}{N}\sum_{i=1}^{3\times 3}\tilde{\mathbf{C}}_{\text{pol},i}\text{trace}\left(\mathbf{C}_{\text{coh}}^{-1}\tilde{\mathbf{C}}_{\text{coh},i}\right). \tag{39}$$

References

[1] N. Bouhlel, V. Akbari, and S. Méric, "Change detection in multilook polarimetric SAR imagery with determinant ratio test statistic," *IEEE Trans. Geosci. Remote Sens.*, vol. 60, 2020, Art. no. 5200515.

[2] V. Akbari, S. N. Anfinsen, A. P. Doulgeris, T. Eltoft, G. Moser, and S. B. Serpico, "Polarimetric SAR change detection with the complex hotelling–Lawley trace statistic," *IEEE Trans. Geosci. Remote Sens.*, vol. 54, no. 7, pp. 3953–3966, Jul. 2016.

[3] S. R. Cloude, *Polarisation: Applications in Remote Sensing*. New York, NY, USA: Oxford Univ. Press, 2009, ch. 3, pp. 115–177.

[4] L. Ferro-Famil, E. Pottier, and J.-S. Lee, "Unsupervised classification of multifrequency and fully polarimetric SAR images based on the H/A/alpha-Wishart classifier," *IEEE Trans. Geosci. Remote Sens.*, vol. 39, no. 11, pp. 2332–2342, Nov. 2001.

[5] S. Tebaldini, "Algebraic synthesis of forest scenarios from multibaseline PolInSAR data," *IEEE Trans. Geosci. Remote Sens.*, vol. 47, no. 12, pp. 4132–4142, Dec. 2009.

[6] E. Blomberg, L. M. H. Ulander, S. Tebaldini, and L. Ferro-Famil, "Evaluating P-band TomoSAR for biomass retrieval in Boreal Forest," *IEEE Trans. Geosci. Remote Sens.*, vol. 59, no. 5, pp. 3793–3804, May 2021.

[7] M. Brandfass, "Generation of bald Earth digital elevation models as applied to polarimetric SAR interferometry," in *Proc. IEEE Int. Geosci. Remote Sens. Symp.*, Jun. 2002, vol. 2, pp. 1014–1016.

[8] T. Shimada, R. Natsuaki, and A. Hirose, "Pixel-by-Pixel scattering mechanism vector optimization in high-resolution PolInSAR," *IEEE Trans. Geosci. Remote Sens.*, vol. 56, no. 5, pp. 2587–2596, May 2018.

[9] L. Pipia et al., "Polarimetric differential SAR interferometry: First results with ground-based measurements," *IEEE Geosci. Remote Sens. Lett.*, vol. 6, no. 1, pp. 167–171, Jan. 2009.

[10] R. Iglesias, D. Monells, X. Fabregas, J. J. Mallorqui, A. Aguasca, and C. Lopez-Martinez, "Phase quality optimization in polarimetric differential SAR interferometry," *IEEE Trans. Geosci. Remote Sens.*, vol. 52, no. 5, pp. 2875–2888, May 2014.

[11] F. Zhao and J. J. Mallorqui, "Coherency matrix decomposition-based polarimetric persistent scatterer interferometry," *IEEE Trans. Geosci. Remote Sens.*, vol. 57, no. 10, pp. 7819–7831, Oct. 2019.

[12] F. Zhao and J. J. Mallorqui, "SMF-POLOPT: An adaptive multitemporal pol(DIn)SAR filtering and phase optimization algorithm for PSI applications," *IEEE Trans. Geosci. Remote Sens.*, vol. 57, no. 9, pp. 7135–7147, Sep. 2019.

[13] A. G. Mullissa, D. Perissin, V. A. Tolpekin, and A. Stein, "Polarimetry-based distributed scatterer processing method for PSI applications," *IEEE Trans. Geosci. Remote Sens.*, vol. 56, no. 6, pp. 3371–3382, Jun. 2018.
[14] S. R. Cloude and K. P. Papathanassiou, "Polarimetric SAR interferometry," *IEEE Trans. Geosci. Remote Sens.*, vol. 36, no. 5, pp. 1551–1565, Sep. 1998.
[15] E. Colin, C. Titin-Schnaider, and W. Tabbara, "An interferometric coherence optimization method in radar polarimetry for high-resolution imagery," *IEEE Trans. Geosci. Remote Sens.*, vol. 44, no. 1, pp. 167–175, Jan. 2006.
[16] M. Tabb, T. Iynn, and R. Carande, "Estimation and removal of SNR and scattering degeneracy effects from the PolInSAR coherence region," in *Proc. IEEE Int. Geosci. Remote Sens. Symp.*, Jul. 2003, pp. 1651–1653.
[17] P. Shen, C. Wang, J. Hu, H. Fu, and J. Zhu, "Interferometric phase optimization based on PolInSAR total power coherency matrix construction and Joint polarization-space nonlocal estimation," *IEEE Trans. Geosci. Remote Sens.*, vol. 60, 2021, Art. no. 5201014.
[18] A. Marino, "Trace coherence: A new operator for polarimetric and interferometric SAR images," *IEEE Trans. Geosci. Remote Sens.*, vol. 55, no. 4, pp. 2326–2339, Apr. 2017.
[19] V. D. Navarro-Sanchez and J. M. Lopez-Sanchez, "Improvement of persistent-scatterer interferometry performance by means of a polarimetric optimization," *IEEE Geosci. Remote Sens. Lett.*, vol. 9, no. 4, pp. 609–613, Jul. 2012.
[20] V. D. Navarro-Sanchez, J. M. Lopez-Sanchez, and L. Ferro-Famil, "Polarimetric approaches for persistent scatterers interferometry," *IEEE Trans. Geosci. Remote Sens.*, vol. 52, no. 3, pp. 1667–1676, Mar. 2014.
[21] Z. Sadeghi, M. J. Valadan Zoej, A. Hooper, and J. M. Lopez-Sanchez, "A new polarimetric persistent scatterer interferometry method using temporal coherence optimization," *IEEE Trans. Geosci. Remote Sens.*, vol. 56, no. 11, pp. 6547–6555, Nov. 2018.
[22] P. Shen, C. Wang, and J. Hu, "A polarization stacking method for optimizing time-series interferometric phases of distributed scatterers," *Remote Sens.*, vol. 14, 2022, Art. no. 4168.
[23] K. Ishitsuka, T. Matsuoka, and M. Tamura, "Persistent scatterer selection incorporating polarimetric SAR interferograms based on maximum likelihood theory," *IEEE Trans. Geosci. Remote Sens.*, vol. 55, no. 1, pp. 38–50, Jan. 2017.
[24] H. Xu, G. Zeng, W. Liu, and Y. Wang, "MLE-MPPL: A maximum likelihood estimator for multipolarimetric phase linking in MTInSAR," *IEEE Trans. Geosci. Remote Sens.*, vol. 61, 2023, Art. no. 5202913.
[25] S. Zwieback and F. J. Meyer, "Reliable InSAR phase history uncertainty estimates," *IEEE Trans. Geosci. Remote Sens.*, vol. 60, 2022, Art. no. 5222109.
[26] S. Zwieback, "Cheap, valid regularizers for improved interferometric phase linking," *IEEE Geosci. Remote Sens. Lett*, vol. 19, 2022, Art. no. 4512704.
[27] J. Zhang, H. Xu, W. Liu, C. Li, and Y. Chen, "Joint design of transmit weight sequence and receive filter for improved target information acquisition in high-resolution radar," *IEEE Trans. Geosci. Remote Sens.*, vol. 60, 2022, Art. no. 5104114.
[28] C.-A. Deledalle, L. Denis, F. Tupin, A. Reigber, and M. Jäger, "NL-SAR: A unified nonlocal framework for resolution-preserving (Pol)(In)SAR denoising," *IEEE Trans. Geosci. Remote Sens.*, vol. 53, no. 4, pp. 2021–2038, Apr. 2015.
[29] H. Xu et al., "A nonlocal noise reduction method based on fringe frequency compensation for SAR interferogram," *IEEE J. Sel. Topics Appl. Earth Observ. Remote Sens.*, vol. 14, pp. 9756–9767, 2021.
[30] A. Ferretti, A. Fumagalli, F. Novali, C. Prati, F. Rocca, and A. Rucci, "A new algorithm for processing interferometric data-stacks: SqueeSAR," *IEEE Trans. Geosci. Remote Sens.*, vol. 49, no. 9, pp. 3460–3470, Sep. 2011.
[31] G. Fornaro, S. Verde, D. Reale, and A. Pauciullo, "CAESAR: An approach based on covariance matrix decomposition to improve multibaseline–Multitemporal interferometric SAR processing," *IEEE Trans. Geosci. Remote Sens.*, vol. 53, no. 4, pp. 2050–2065, Apr. 2015.
[32] N. Cao, H. Lee, and H. C. Jung, "A phase-decomposition-based PSInSAR processing method," *IEEE Trans. Geosci. Remote Sens.*, vol. 54, no. 2, pp. 1074–1090, Feb. 2016.
[33] H. Ansari, F. De Zan, and R. Bamler, "Efficient phase estimation for interferogram stacks," *IEEE Trans. Geosci. Remote Sens.*, vol. 56, no. 7, pp. 4109–4125, Jul. 2018.
[34] J.-S. Lee, S. R. Cloude, K. P. Papathanassiou, M. R. Grunes, and I. H. Woodhouse, "Speckle filtering and coherence estimation of polarimetric SAR interferometry data for forest applications," *IEEE Trans. Geosci. Remote Sens.*, vol. 41, no. 10, pp. 2254–2263, Oct. 2003.
[35] M. Neumann, L. Ferro-Famil, and A. Reigber, "Multibaseline polarimetric SAR interferometry coherence optimization," *IEEE Geosci. Remote Sens. Lett.*, vol. 5, no. 1, pp. 93–97, Jan. 2008.
[36] R. F. Hanssen, *Radar Interferometry: Data Interpretation and Error Analysis*. Dordrecht, The Netherlands: Kluwer, 2001.
[37] R. Scheiber and A. Moreira, "Coregistration of interferometric SAR images using spectral diversity," *IEEE Trans. Geosci. Remote Sens.*, vol. 38, no. 5, pp. 2179–2191, Sep. 2000.
[38] N. Cao, H. Lee, and H. C. Jung, "Mathematical framework for phase-triangulation algorithms in distributed-scatterer interferometry," *IEEE Geosci. Remote Sens. Lett.*, vol. 12, no. 9, pp. 1838–1842, Sep. 2015.
[39] D. H. T. Minh and S. Tebaldini, "Interferometric phase linking: Algorithm, application, and perspective," *IEEE Geosci. Remote Sens. Mag.*, vol. 11, no. 3, pp. 46–62, Sep. 2023.

Guobing Zeng received the B.S. degree in aircraft engineering from Beihang University, Beijing, China, in 2019. He is currently working toward the Ph.D. degree in signal and information processing with the School of Electronic and Information Engineering, Beihang University.

His current research interests include SAR interferometry, differential SAR interferometry, polarimetric differential SAR interferometry, and polarimetric SAR tomography.

Huaping Xu (Member, IEEE) received the B.S. degree in electronic engineering and the Ph.D. degree in communication and information system from Beihang University, Beijing, China, in 1998 and 2003, respectively.

She is currently a Professor with the School of Electronic and Information Engineering, Beihang University. Her current research interests include synthetic aperture radar (SAR) interferometry, differential SAR interferometry, image processing, and radar waveform design. She has authored or coauthored more than 100 journal and conference papers, and a research monograph about signal processing.

Wei Liu (Senior Member, IEEE) received the B.Sc. degree in space physics and the L.L.B. degree in intellectual property law from Peking University, Beijing, China, in 1996 and 1997, respectively, the M.Phil. degree from the Department of Electrical and Electronic Engineering, University of Hong Kong, Hong Kong, in 2001, and the Ph.D. degree from the School of Electronics and Computer Science, University of Southampton, Southampton, U.K., in 2003.

He worked as a Postdoc first at Southampton and later with Imperial College London. In September 2005, he joined the Department of Electronic and Electrical Engineering, University of Sheffield, U.K., first as a Lecturer and then a Senior Lecturer. Since 2023, he has been a Reader with the School of Electronic Engineering and Computer Science, Queen Mary University of London, London, U.K.. He has authored and coauthored 390+ journal and conference papers, 5 book chapters, and 2 research monographs titled *Wideband Beamforming: Concepts and Techniques* (Wiley, March 2010) and *Low-Cost Smart Antennas* (Wiley, March 2019), respectively. His research interests include a wide range of topics in signal processing, with a focus on sensor array signal processing and its various applications, such as robotics and autonomous systems, human computer interface, radar, sonar, and wireless communications.

Dr. Liu is a member of the Digital Signal Processing Technical Committee of IEEE Circuits and Systems Society (Chair from May 2022) and the Sensor Array and Multichannel Signal Processing Technical Committee of IEEE Signal Processing Society (Chair for 2021–2022), and an IEEE Distinguished Lecturer for the Aerospace and Electronic Systems Society (2023–2024). He also acted as an Associate Editor for IEEE TRANSACTIONS ON SIGNAL PROCESSING, IEEE ACCESS, and *Journal of the Franklin Institute* (2021–2023), and currently is an Executive Associate Editor-in-Chief of the *Frontiers of Information Technology and Electronic Engineering*.

Aifang Liu was born in Wuxiang, Shanxi, China, in 1974. He received the B.S. degree in electronic engineering from Shanxi University, Taiyuan, China, in 1997, and the M.S. and Ph.D. degrees in communication and information system from the Nanjing University of Science and Technology, Nanjing, China, in 2001 and 2004, respectively.

He is currently with the Nanjing Research Institute of Electronics Technology, Nanjing, and is mainly engaged in the design of space-based radar system and synthetic aperture radar system.

Yuan Wang received the B.S. degree in automation from the School of Information and Communication Engineering, Communication University of China, Beijing, China, in 2019. She is currently working toward the Ph.D. degree in signal and information processing with the School of Electronic and Information Engineering, Beihang University, Beijing.

Her current research interests include synthetic aperture radar (SAR) interferometry, and interferometric SAR image processing.